



Multilayer graphane synthesized under high hydrogen pressure



V.E. Antonov^{a, *}, I.O. Bashkin^a, A.V. Bazhenov^a, B.M. Bulychev^b, V.K. Fedotov^a,
T.N. Fursova^a, A.I. Kolesnikov^c, V.I. Kulakov^a, R.V. Lukashev^d, D.V. Matveev^a,
M.K. Sakharov^a, Y.M. Shulga^e

^a Institute of Solid State Physics RAS, 142432, Chernogolovka, Moscow District, Russia

^b Moscow State University, Leninskie Gory, 119992 Moscow, Russia

^c Chemical and Engineering Materials Division, Oak Ridge National Laboratory, Oak Ridge, TN 37831, USA

^d Institute of Problems of Chemical Physics RAS, 142432, Chernogolovka, Moscow District, Russia

^e National University of Science and Technology 'MISIS', Leninsky Pr. 4, 119049 Moscow, Russia

ARTICLE INFO

Article history:

Received 20 August 2015

Received in revised form

15 December 2015

Accepted 17 December 2015

Available online 19 December 2015

ABSTRACT

A new hydrocarbon – hydrographite – with the composition close to CH is shown to form from graphite and gaseous hydrogen at pressures above 2 GPa and temperatures from 450 to 700 °C. Hydrographite is a black solid thermally stable under ambient conditions. If heated in vacuum, it decomposes into graphite and molecular hydrogen at temperatures from 500 to 650 °C. Powder X-ray diffraction characterizes hydrographite as a multilayer “graphane II” phase predicted by *ab initio* calculations [Wen X-D et al. PNAS 2011; 108:6833] and consisting of graphane sheets in the chair conformation stacked along the hexagonal c axis in the –ABAB– sequence. The crystal structure of the synthesized phase belongs to the P6₃mc space group. The unit cell parameters are $a = 2.53(1)$ Å and $c = 9.54(1)$ Å and therefore exceed the corresponding parameters of graphite by 2.4(2)% and 42.0(3)%. Stretching vibrations of C–H groups on the surface of the hydrographite particles are examined by infrared spectroscopy.

© 2015 Published by Elsevier Ltd.

1. Introduction

The past decades have demonstrated the effectiveness of high pressures for the synthesis of hydrocarbons. In particular, exposing different carbon and hydrogen donors to the *T-P* conditions characteristic of the Earth's upper mantle (pressures of a few GPa and temperatures of up to 1500 °C) resulted in the abiogenic synthesis of methane [1] and a hydrocarbon mixture [2,3] similar in composition to the hydrocarbon part of the natural gas. Exposing single-wall carbon nanotubes (SWNTs) and graphite nanofibres (GNFs) to a hydrogen atmosphere at $P = 9$ GPa and $T = 450$ °C gave hydrocarbons never observed before [4].

These new hydrocarbons are black solids having H/C atomic ratios of up to $x \approx 0.85$. Unlike the commonly studied SWNTs and GNFs with physisorbed H₂ molecules easily leaving the samples at room and even liquid nitrogen temperature (see, e.g., review [5]), the new hydrocarbons are thermally stable. Particularly, the hydrogenated GNFs heated in vacuum at 20 °C/min begin evolving H₂

at 500 °C, and the complete removal of the hydrogen requires annealing at 700 °C [4]. An X-ray diffraction study showed that the hydrogenation of GNFs increases the interplanar spacing between their graphene layers by approximately 40%, from 3.36 to 4.67 Å. The IR spectroscopy characterised the hydrogenated GNFs as mostly covalent compounds with two narrow vibrational bands at 2860 and 2920 cm⁻¹, i.e., in the energy range typical of stretching C–H vibrations [4].

In view of these findings, synthesis of hydrogenated crystalline graphite was a challenge. However, we failed to prepare it at H₂ pressures as high as 9 GPa and temperatures up to 450 °C using plates of bulk graphite and graphite flakes as the starting materials.

At the same time, graphite was known to absorb hydrogen up to $x = 0.95$ in the course of amorphization under intense ball milling (80 h at 400 rpm) at an H₂ pressure of only 1 MPa [6]. In order to activate the surface of the graphite without destroying its crystallinity, we ball milled its bulk pieces under rather mild conditions (30 min at 250 rpm in Ar). Exposing the resulting graphite powder to H₂ pressures of 4–7 GPa at 450 °C for a period of 24 h gave samples with the mean hydrogen content varying from $x = 0.66$ to 0.94. The samples were composed of a mixture of a new crystalline hydrocarbon with $x \approx 1$ (hydrographite for short) and unreacted

* Corresponding author.

E-mail address: antonov@issp.ac.ru (V.E. Antonov).

graphite. The thermal stability, the spacing between the graphene layers and the energies of the stretching C–H modes in the synthesized hydrographite proved to be similar to those of the hydrogenated GNFs. A single-phase sample of deuterated graphite with D/C = 1.06(5) was also produced and examined. In 2007, these preliminary results were briefly reported in Ref. [7].

All of a sudden, further studies of hydrographite were hampered by irreproducibility of its synthesis. After the first batch of the mechanically activated graphite was consumed, our attempts to prepare a new portion of such graphite using the same starting material and the same procedure of ball milling only gave powders that could be hydrogenated to $x \approx 0.2$. It was only recently that we have been able to raise the synthesis temperature to 700 °C and began consistently producing samples with $x \approx 0.6$ –0.7.

Meanwhile, the discovery of graphene (a flat monolayer of carbon atoms) [8,9] triggered a considerable interest to the synthesis of chemically modified carbon sheets. It was proposed that graphane, representing a graphene sheet saturated by hydrogen adsorbed from both sides, would be stable [10,11], and such a material was soon synthesized and experimentally studied [12]. There were extensive computer simulations [13–22] for the structure, electronic and vibrational properties of a single layer and bilayer graphane and also of a multilayer, bulk crystalline graphane. The principal conclusion was (see, e.g., Ref. [18]) that “a 3D graphane system might eventually be synthesized.”

The hydrographite obtained in our experiments is likely to be this very 3D graphane system. The present paper discusses results of [7] in more detail, reports on our recent findings concerning the crystal structure of hydrographite and its stability at high hydrogen pressures and elevated temperatures and also provides a more likely interpretation of its IR spectra.

2. Experimental

The starting material was high-purity electrode graphite containing: 4×10^{-5} wt.% Fe; 1×10^{-4} wt.% Si; 2×10^{-5} wt.% Ca and less than 1×10^{-5} wt.% of B, Mg, Mn, Al, Ti, Cu, V, Ni and Ag. About 2 g of this graphite together with a few stainless steel balls 10 mm in diameter were placed in a 250 cm³ stainless steel vial and ball-milled for 30 min at a rotation speed of 250 rpm under an Ar atmosphere at room temperature using a planetary ball mill Fritsch Pulverisette 6.

To synthesize hydrographite, 100 mg batches of this mechanically activated graphite powder were exposed to an atmosphere of gaseous hydrogen at fixed pressures ranging from 0.6 to 7.5 GPa and temperatures from 350 to 800 °C for periods varying from 24 h at 350 °C to 30 min at 800 °C. The hydrogen was produced inside the high-pressure cell using thermal decomposition of an internal hydrogen source, AlH₃ or NH₃BH₃, incased into a tightly plugged copper capsule together with the graphite powder and separated from it by a thin layer of Pd (the method is described in more detail in Ref. [23]; the experiments were carried out using a quasihydrostatic Toroid-type high-pressure chamber [24]). After the hydrogenation was complete, the sample was cooled to 80 K or to room temperature, recovered to the ambient pressure and further stored in liquid nitrogen until the measurements.

A few samples of deuterated graphite were produced in a similar way using AlD₃ as the internal deuterium source in the high-pressure cell. This aluminium deuteride was slightly contaminated with protium and had an atomic ratio of H/(D + H) = 0.029(2) according to mass-spectrometry [25].

The hydrogen evolution from the prepared C–H samples and the total hydrogen content of these samples were examined by thermodesorption of the gas into a pre-evacuated measuring

system in the regime of heating to 660 °C at rates of 10 or 20 °C/min. The amount of hydrogen remaining in the samples after a one day exposure to room temperature was also determined for a few samples by combustion in a flow of oxygen at 1400 °C followed by weighting the resultant CO₂ and H₂O (analyzer “Vario Micro Cube”, Elementar GmbH). In both methods, the mean H/C atomic ratio was measured with a relative accuracy of 5%.

Samples of the initial and hydrogenated and dehydrogenated graphite were studied at room temperature by powder X-ray diffraction using a Siemens D500 diffractometer with Cu K α radiation selected by a diffracted beam monochromator. Atomic vibrations in these substances were characterized by IR transmission spectra measured at room temperature with a Bruker IFS-113v Fourier spectrometer in the range 400–5000 cm⁻¹ with a resolution of 4 cm⁻¹. The samples for the IR spectroscopy were in the form of pellets pressed from mixtures of a powder of the initial or hydrogenated graphite with a powder of KBr.

3. Results and discussion

3.1. Hydrogen content and thermal stability of quenched samples of hydrographite

To estimate the thermodesorption characteristics of the graphite–H samples synthesized under high hydrogen pressures, a 0.5–5 mg portion of the quenched sample was first encased into a thin-wall non-hermetic copper container submerged in liquid nitrogen. The container was then dropped to the bottom of a quartz ampoule cooled by liquid nitrogen from outside. The ampoule, with its lower end still submerged in the nitrogen bath, was vertically attached to the measuring system and the system was pumped out to a pressure of 2×10^{-3} Torr. After that, the lower part of the quartz ampoule with the incased sample was heated at a rate of 20 or 10 °C/min and the amount of the gas releasing from the sample was determined from the pressure in the system.

Fig. 1A shows typical desorption curves for the graphite–H and graphite–D samples. The curves are constructed assuming that the evolved gas was molecular hydrogen (deuterium). Fig. 1B compares a curve for the hydrogenated graphite measured at 20 °C/min with those for the hydrogenated graphite nanofibres and single-walled nanotubes measured earlier [4] at the same heating rate.

As seen from Fig. 1, the desorption curves for the hydrogenated graphite, GNFs and SWNTs look similar and the gas release is a two-stage process. In heating the sample from 77 K to approximately room temperature, the amount of the liberated gas gradually increases, reaches a rather small but still reliably detectable atomic H/C ratio of $x \approx 0.02$ –0.05 and nearly stops changing. Most hydrogen is evolved at the second stage that starts above 500 °C and stops around 650 °C.

The occurrence of the two well-separated stages in the thermodesorption curves suggests that the quenched hydrocarbons contain hydrogen in two different forms. In the case of the quenched SWNT–H sample with $x \approx 0.61$ synthesized at 3 GPa and 350 °C, these two forms of the absorbed hydrogen have been identified by inelastic neutron scattering [26]. The weakly bonded hydrogen ($x \approx 0.05$) leaving the sample upon heating to room temperature was shown to be the physisorbed H₂ molecules exhibiting nearly free rotational behaviour, while most H atoms ($x = 0.56$) were covalently bound to the carbon atoms and could only be removed by heating to $T > 500$ °C. The two forms of hydrogen contained in our samples of hydrogenated graphite and GNFs are likely to be the same. This paper will further deal with the covalently bound hydrogen remaining in the samples under ambient conditions, and the hydrogen content of the samples will refer to this hydrogen only.

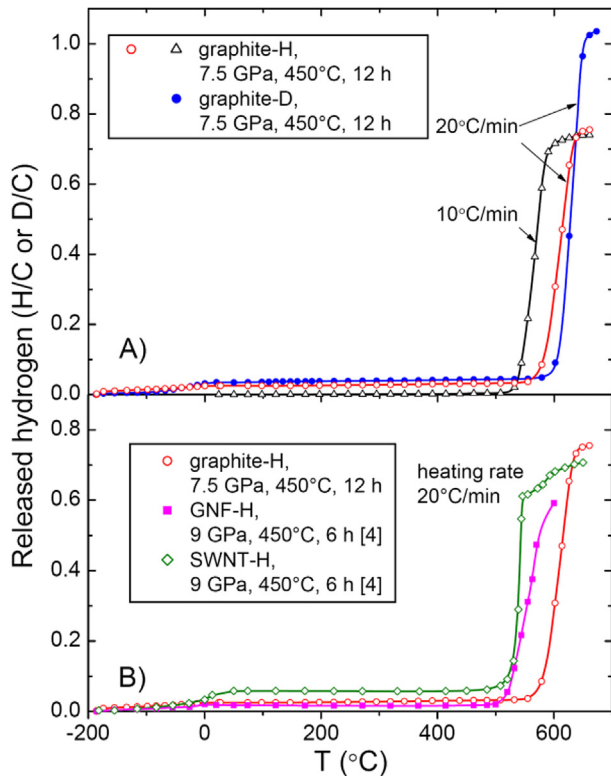


Fig. 1. Temperature dependences of the amount of hydrogen (deuterium) released from quenched graphite-H and graphite-D samples (results of the present work) and GNF-H and SWNT-H samples (results of [4]) heated at a rate of 20 or 10 °C/min in a closed-volume, pre-evacuated measuring system. The gas pressures and temperature of the sample synthesis are indicated in the legends to the symbols. The dependence shown in (A) by open triangles is for the graphite-H sample preliminarily exposed to room temperature for 1 day. (A colour version of this figure can be viewed online.)

Our assumption that the high-pressure hydrocarbons heated in vacuum above 500 °C should emit molecular hydrogen nearly free of volatile hydrocarbons like CH₄, C₂H₆, etc., was based on results for the hydrogenated SWNTs studied by mass spectrometry [27]. To check if this is also true for hydrographite, we analyzed a few graphite-H and graphite-D samples by combustion in an oxygen flow at 1400 °C. The analysis of 2 mg portions of the samples exposed to ambient conditions for one day gave virtually the same contents of the covalently bonded hydrogen as the thermodesorption did. For example, the graphite-D sample that released $x \approx 1.04\text{--}0.04 = 1.00(5)$ of deuterium in heating from room temperature to 670 °C (see Fig. 1A) was shown to have $x = 1.06(5)$ by the combustion analysis. Such an agreement evidences that in the thermodesorption experiments:

- nearly all hydrogen was evolved in the form of H₂ molecules rather than gaseous hydrocarbons (e.g., if methane CH₄ were released, the number of its molecules and, correspondingly, the pressure would be twice as low);
- nearly all hydrogen was evolved at temperatures below 650 °C (otherwise, the combustion at 1400 °C would detect more hydrogen than the thermodesorption).

It seems worth mentioning in this connection that another graphite-based hydrocarbon, the nanostructured material with $x \approx 0.95$ produced by intensive ball-milling of graphite in an H₂ atmosphere [6], was also thermally stable. According to the mass spectra measured in Ref. [28], it also evolved nearly pure H₂ when

heated in vacuum. At the same time, the kinetics of the hydrogen desorption from the nanostructured material were quite different. This material released hydrogen in two steps starting at ≈ 330 and ≈ 680 °C, respectively [28], whereas the crystalline hydrographite and other high-pressure hydrocarbons evolved most hydrogen in one step starting at 500–600 °C (see Fig. 1). The origin of the first step in the desorption curve of the nanostructured graphite is not well understood. The second step occurred near the recrystallization temperature of the studied samples and it was tentatively attributed to the release of the hydrogen atoms trapped at carbon dangling bonds [28].

As for the kinetics of hydrogen desorption from the crystalline hydrographite, the position and width of the temperature interval of the intensive hydrogen release proved to be mostly insensitive to the type of the hydrogen isotope, protium or deuterium (compare the curves in Fig. 1A for the graphite-D and graphite-H samples measured at 20 °C/min). A decrease in the heating rate from 20 to 10 °C/min lowered the starting temperature of the hydrogen release by 30–50 °C, from about 560 to 520 °C (compare the dependences in Fig. 1A for two different portions of the same graphite-H sample). A one day vacuum annealing of a graphite-H sample at 450 °C only resulted in the desorption of a few per cent of its total hydrogen content. Compared to other high-pressure hydrocarbons, GNF-H and SWNT-H, hydrographite is a little more thermally stable (see Fig. 1B).

3.2. Crystal structure of hydrographite

Fig. 2 shows an X-ray diffraction pattern of the initial ball-milled graphite, which was further used to synthesize the graphite-H and graphite-D samples under high gas pressures. The considerable broadening of the 00 ℓ lines toward low angles is typical of the ball-milled graphite [29,30] and mainly results from fracturing the graphite particles and the formation of stacking faults, dangling bonds and other defects. The shape of the 002 line can roughly be described by the approximately equal contributions from two types of grains with the P6₃/mmc structure. These are the crystallites with $a = 2.47$ Å, $c = 6.72$ Å and the coherence length $L_c = 13$ nm in the direction of the hexagonal axis (thin solid curve in Fig. 2) and nanocrystals with $a = 2.50$ Å, $c = 7.10$ Å and $L_c = 4$ nm (the dashed

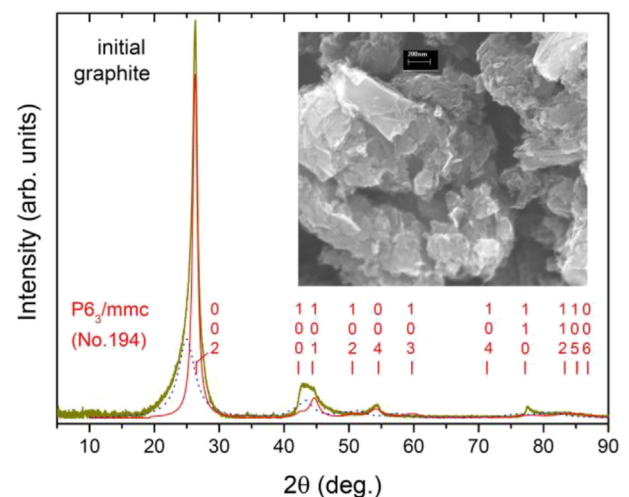


Fig. 2. X-ray diffraction pattern of the ball-milled graphite used to synthesize the graphite-H and graphite-D samples [7]. Room temperature, Cu K α radiation. The smooth background is subtracted. The inset shows an SEM image obtained from the same graphite powder using a high-resolution scanning electron microscope Zeiss Supra 50 VP. (A colour version of this figure can be viewed online.)

curve). The coherence lengths are estimated using Scherrer's equation $L_c = 1.5\lambda/(\Delta \cdot \cos\theta)$, where λ is the wavelength of the Cu $K\alpha$ radiation and θ and Δ are, respectively, the angle and the half-width at half-maximum of the 002 peak.

As seen from the SEM micrograph in the inset in Fig. 2, our ball-milled graphite was composed of agglomerated platelets typical of graphite powders (SEM images of the hydrogenated samples looked similar). The surface of these platelets is parallel to the ab-planes of the hexagonal crystal lattice of graphite and perpendicular to the c-axis. The dimensions of the platelets reach $200 \times 400 \text{ nm}^2$ and therefore exceed the coherence length L_c in the c-direction by an order of magnitude. Correspondingly, the reciprocal lattice sites should be shaped like rods oriented along the reciprocal c^* -axis. This suggests that the width of the lines in the diffraction pattern of such a powder should strongly depend on their Miller indices. As a result, profile analysis of diffraction patterns of the initial and hydrogenated graphite samples could only be performed on a semi-quantitative level in the present paper.

The bottom spectrum in Fig. 3 represents an X-ray diffraction pattern of a single-phase sample of deuterated graphite with the composition $CD_{1.06(5)}$. The most prominent feature of this pattern is a shift of the 002 diffraction line of graphite to lower angles corresponding to the approximately 42% increase in the c-parameter of the hexagonal lattice of graphite, from 6.72 to 9.54 Å. The line also becomes less broadened from the left-hand side. Presumably, this is due to the partial annealing of defects in the course of hydrogenation of the ball-milled graphite at an elevated temperature of 450 °C. Using Scherrer's equation, the width of the 002 line gives the coherence length $L_c = 10 \text{ nm}$.

After the $CD_{1.06}$ sample is fully outgassed at 600 °C in vacuum, the width of its 002 line further decreases and corresponds to $L_c = 14 \text{ nm}$ (the upper spectrum in Fig. 3). The lattice parameters of the degassed sample revert to those of the fraction with $L_c = 13 \text{ nm}$ in the initial graphite and the X-ray patterns of both the initial (Fig. 2) and degassed (Fig. 3) graphite samples can satisfactorily be described in the $P6_3/mmc$ space group. The structural parameters resulted from the (semi-quantitative) profile analysis of the diffraction pattern of the outgassed sample are presented in Table 1. We chose this sample as the reference state of the non-

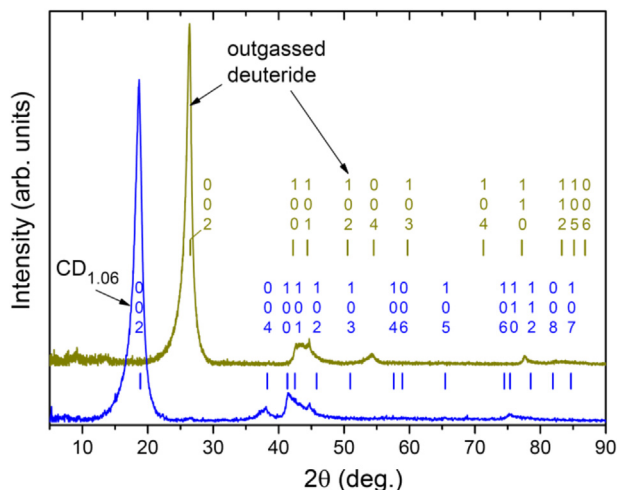


Fig. 3. X-ray diffraction pattern of the graphite-D sample with D/C = 1.06(5) synthesized at a D_2 pressure of 7.5 GPa and $T = 450 \text{ °C}$ [7] (the bottom spectrum) and a pattern of the same sample after the complete removal of deuterium by a 4 h annealing at 600 °C in vacuum (the spectrum is shifted upwards). Room temperature, Cu $K\alpha$ radiation, subtracted background. (A colour version of this figure can be viewed online.)

Table 1

Structural parameters of the graphite-D sample with D/C = 1.06(5) and of pure graphite produced by outgassing this graphite-D sample at 600 °C in vacuum. The parameters are obtained by a profile analysis of the X-ray diffraction patterns of these samples presented in Fig. 3. Positions of the D atoms could not be reliably determined from experiment and these atoms are placed at a distance of $0.12c \approx 1.1 \text{ Å}$ in the c-direction from the nearest C atom in accordance with results of most *ab initio* calculations for the chair conformation of graphane.

Sample	Graphite (outgassed)	Graphite-D
D/C atomic ratio	0	1.06(5)
Space group	$P6_3/mmc$ (no. 194)	$P6_3mc$ (no. 186)
Positions of C atoms	$2c$ (1/3, 2/3, 1/4)	2a (0, 0, 0) 2b (1/3, 2/3, 0.05) 2a (0, 0, 0.88) 2b (1/3, 2/3, 0.17)
Tentative positions of D atoms		Increase (%)
a (Å)	2.47(1)	2.53(1) 2.4(2)
c (Å)	6.72(1)	9.54(1) 42.0(3)
c/a	2.72(1)	3.77(2) 39(1)
V (Å ³ /atom C)	35.5(3)	52.9(4) 49(2)

hydrogenated graphite, because comparison of the hydrogenated graphite with the starting graphite would be more ambiguous due to the much stronger and asymmetrical broadening of its diffraction lines.

The diffraction pattern of the deuterated sample $CD_{1.06}$ was modeled on the basis of a graphite-like crystal structure (space group $P6_3/mmc$) and the structures of the two forms of multilayer graphane, “graphane I” and “graphane II”, which are most stable at $T = 0 \text{ K}$ and pressures below 10 GPa according to the *ab initio* calculations of Ref. [18]. The structure of “graphane I” belongs to the $P3m1$ space group (in Ref. [18], it was misprinted as $P\bar{3}m1$) and the space group of “graphane II” is $P6_3mc$. The resulting profile fits are shown in Fig. 4.

As seen from Fig. 4, the intensity distribution among the diffraction lines in the angular range $30 < 2\theta < 50^\circ$ can semi-quantitatively be reproduced in the $P6_3mc$ space group, whereas the $P6_3/mmc$ and $P3m1$ groups give qualitatively inadequate distributions. The inapplicability of the $P6_3/mmc$ group is not surprising, because none of the *ab initio* calculations has ever predicted a graphite-like structure for a single layer or bilayer or multilayer graphane. As for the predicted $P3m1$ and $P6_3mc$ structures [18], they are built from similar CH graphane layers in the chair conformation and only differ from each other by the stacking sequences of these layers along the c-axis. Namely, these are the –AAAA– sequence in the case of the $P3m1$ phase and –ABAB– sequence for the $P6_3mc$ phase.

Due to the weak interactions between the layers in a graphane crystal, the differences in the calculated enthalpies [18] of the $P3m1$ and $P6_3mc$ stacking polymorphs were too small to determine which of these phases is more stable at $T = 0 \text{ K}$ and pressures up to 120 GPa. Our X-ray results (Fig. 4) are in favour of the $P6_3mc$ structure of the $CD_{1.06}$ phase. We think that $P6_3mc$ is the most likely structure of this phase because all other possible forms of multilayer graphane are considerably less stable than the $P3m1$ and $P6_3mc$ ones at pressures up to 10 GPa [18], while our $CD_{1.06}$ sample was synthesized at a lower pressure of 7.5 GPa and studied by X-ray diffraction at ambient pressure.

Refined parameters of the $P6_3mc$ structure of the $CD_{1.06}$ phase (“graphane II” structure according to Ref. [18]; –ABAB– stacking; 4 CD pairs in the unit cell) are listed in the rightmost column of Table 1. As one can see, the hydrogenation of graphite resulted in the increase of its atomic volume by nearly 50%, and this increase was mostly due to the elongation of the c-parameter by 42%.

A schematic representation of the $P6_3mc$ structure of such a graphane crystal is given in Fig. 5. This is the so-called “buckled”

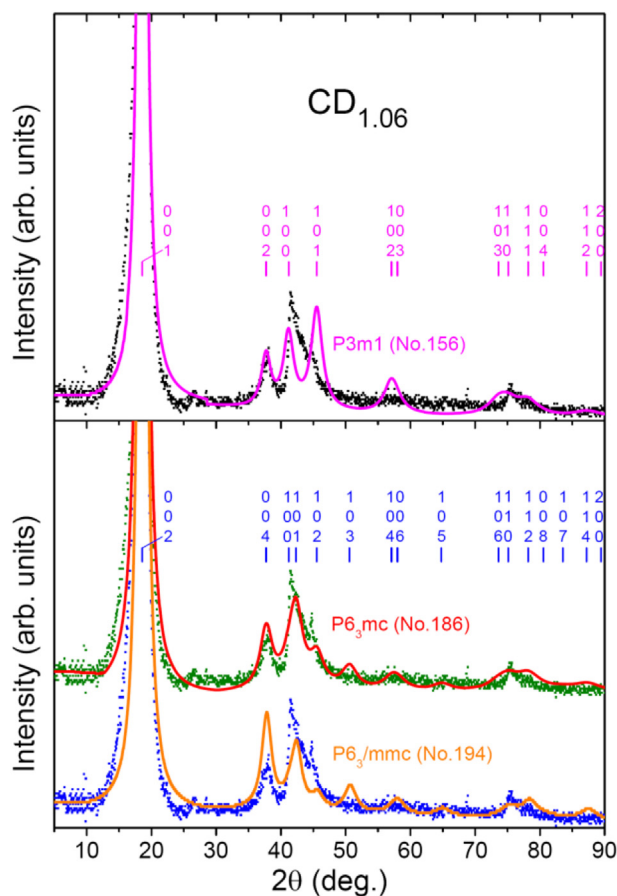


Fig. 4. Experimental X-ray pattern of the $CD_{1.06}$ sample (solid squares; the same data as in Fig. 3) and results of its semi-quantitative profile analysis in the framework of the $P6_3/mmc$ and $P3m1$ space groups (solid curves). The c -parameter of the $P3m1$ structure is twice as small as that of the $P6_3/mmc$ and $P6_3/mc$ structures. (A colour version of this figure can be viewed online.)

structure composed of weakly coupled single graphane layers in the chair conformation, in which every alternate carbon atom is attached to the hydrogen atom from alternate sides of the plane and displaced out of the hexagonal plane (buckled) toward this hydrogen atom. The profile refinement gave a value of $\delta z \approx 0.05c/2 \approx 0.25 \text{ \AA}$ for the displacement in the $CD_{1.06}$ compound (see Table 1). Such a displacement leads to the significantly increased minimum distance $d_{C-C} = 1.54 \text{ \AA}$ between the neighboring carbon atoms in the buckled structure compared with $d_{C-C} = a/\sqrt{3} \approx 1.46 \text{ \AA}$ in a flat carbon layer ($\delta z = 0$) with the same lattice parameter $a = 2.53 \text{ \AA}$. The distance $d_{C-C} = 1.54 \text{ \AA}$ agrees with predictions of most *ab initio* calculations (see, e.g., [13,18]) thus favoring the chair conformation of the graphane layers chosen to model the $CD_{1.06}$ structure.

The experimental interplanar distance $c/2 = 4.77(1) \text{ \AA}$ in the $CD_{1.06}$ sample agrees with the predicted distance between the graphane layers in multilayer graphane: 4.978 \AA [11]; $5\text{--}6 \text{ \AA}$ [13] and $4.5\text{--}4.8 \text{ \AA}$ [19]. All *ab initio* calculations also predict that the in-plane parameter, a , of the single-, bi- and multilayer graphane in the chair conformation should be larger than $a_0 \approx 2.47 \text{ \AA}$ of graphite. In the case of the multilayer graphane, the calculations give $a = 2.516 \text{ \AA}$ [11] and $a = 2.545 \text{ \AA}$ [13]. The experimental value of $a = 2.53(1) \text{ \AA}$ for our $CD_{1.06}$ sample lies in between the predicted values.

The calculations for multilayer graphanes also showed that the in-plane periodicity in the graphane layers is virtually insensitive to

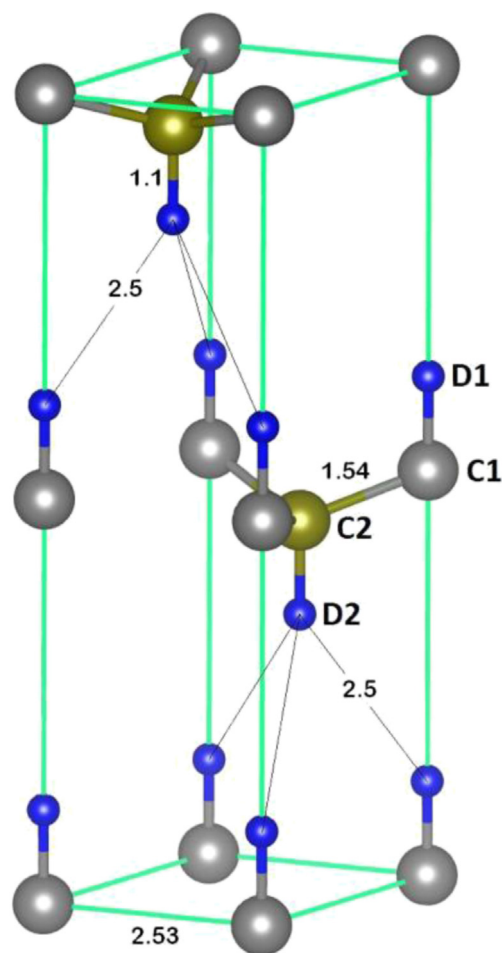


Fig. 5. The $P6_3/mc$ structure of a graphane crystal (see Table 1). Large spheres represent C atoms; small spheres stand for D atoms. The atoms labeled C1 and D1 sit on the 2a positions; those labeled C2 and D2 are on the 2b positions. Numbers indicate the interatomic distances in Angstroms. (A colour version of this figure can be viewed online.)

the weak interaction between different layers. Therefore, the stable chair conformation of the single-layer graphane is likely to have a $\approx 2.53 \text{ \AA}$ in accordance with both the calculations and our experimental result for hydrographite. At the same time, most samples of the single-layer graphane synthesized in Ref. [12] had the in-plane periodicity (called the d -parameter), which was smaller by 1–5% than $a_0 \approx 2.47 \text{ \AA}$ of graphite. We think it was a non-equilibrium result. A discussion of its possible origin can be found in Ref. [13].

3.3. Formation and decomposition of hydrographite under high hydrogen pressure

The $CD_{1.06}$ sample discussed above was the only single-phase sample of multilayer graphane examined in the present work. X-ray diffraction studies of a few dozens of other graphite-D and graphite-H samples synthesized at pressures from 2.5 to 7.5 GPa and temperatures $350\text{--}700 \text{ }^\circ\text{C}$ showed them to consist of a two-phase mixture of unreacted graphite and a hydrographite phase with the same lattice parameters as those of the $CD_{1.06}$ phase. The unreacted fraction of the samples was usually composed of the largest grains and its 002 line was clearly visible in the diffraction patterns. Particularly, such a line was seen in the pattern of the graphite-H sample with the mean atomic ratio $H/C = 0.94(5)$. We therefore conclude that the high-pressure hydrogenation of

graphite always proceeded as a two-phase reaction and the final product of this reaction was a multilayer graphane with the composition close to CH.

Fig. 6 shows the maximal yield of hydrographite at 450 °C estimated by the ratio of intensities of the strongest 002 lines of hydrographite and unreacted graphite in the studied graphite-H samples. As one can see, hydrographite was only formed at hydrogen pressures above 2 GPa.

Exposing the ball-milled graphite for a few hours to a hydrogen pressure of 7.5 GPa at temperatures from 530 to 630 °C gave samples with H/C = 0.6–0.7, which contained, correspondingly, 60–70 mol.% hydrographite. An increase in the synthesis temperature to 700 °C did not increase the yield of hydrographite and at temperatures above 720 °C, hydrographite did not often form at all.

To examine the decomposition conditions of hydrographite at an H₂ pressure of 7.5 GPa, we used a graphite-H sample synthesized at 7.5 GPa and 530 °C and weighing about 100 mg. The sample had H/C = 0.69 and consisted of a mixture of approximately 69 mol.% hydrographite and 31 mol.% unreacted graphite. Exposing small portions (about 3 mg) of this sample to the hydrogen pressure 7.5 GPa and temperatures up to 630 °C resulted in an increase in their hydrogen content. At 700 °C, the H/C ratio remained virtually unchanged. At 720–750 °C, it did not change in some samples and decreased to H/C ≈ 0.02–0.03 in some other samples. At T ≥ 775 °C, the hydrogen content of all studied samples decreased to H/C ≈ 0.02–0.03. In addition, the samples with this small hydrogen content lost about 2/3 of their initial mass.

The most plausible explanation of the observed effects is that under a hydrogen pressure of 7.5 GPa, hydrographite remains stable in respect to the decomposition into graphite and molecular H₂ at temperatures up to about 720 °C. However, starting with this temperature, hydrographite becomes thermally unstable relative to the formation of methane and/or other light hydrocarbons. These hydrocarbons are fluids under the experimental conditions and they mostly leave the sample and mix with the hydrogen gas and sop in the debris of the high-pressure cell. The carryover of about 69 mol.% hydrographite from the solid sample leads to the loss of approximately 2/3 of its overall mass and this is what the experiment shows. The 31 mol.% of the unreacted graphite contained in the starting sample remains intact, because the synthesis of

methane and other light hydrocarbons from graphite and H₂ requires higher temperatures due to the slow kinetics of the process (see, e.g., [1–3]).

3.4. Infrared spectra of hydrographite

Fig. 7 presents IR transmission spectra of our ball-milled graphite and the samples of hydrogenated and deuterated graphite with the maximal H or D concentrations. As discussed in Section 3.2, X-ray diffraction showed the CD_{1.06} sample to be single-phase hydrographite. The CH_{0.94} sample contained a few percent of unreacted graphite (the composition of this sample is indicated by the rightmost point in Fig. 6). Prior to each IR measurement, a portion of 0.014 mg of a powdered sample was mixed with 80 mg of KBr powder and compacted at a pressure of 0.7 GPa into pellets with a diameter of 6 mm and thickness of 0.5 mm. Using the similarly prepared pellets allowed a direct comparison of the light transmission by the studied samples.

The IR spectrum of the graphite powder shows a monotonic decrease in the light transmittance T with increasing photon frequency ν . Such a featureless IR spectrum is typical of the ball-milled graphite [31]. The spectra of the CH_{0.94} and CD_{1.06} samples demonstrate a similar overall monotonic decrease in the light transmittance with increasing photon energy together with the appearance of narrow absorption bands in the energy range characteristic of the stretching C–H and C–D vibrations in hydrocarbons.

As one can see from Fig. 7, within the whole studied energy range, the total light transmittance of CH_{0.94} and CD_{1.06} is approximately 2 and 4 times higher than that of the graphite. Light transmittance of a conducting powder is mostly determined by the light scattering on small particles and by the light absorption by free charge carriers in these particles [32]. The monotonic decrease in the light transmittance with increasing photon energy observed in each of the three studied samples is characteristic of scattering on the particles with the dimensions of the order of or less than the wavelength of the incident light. The studied range $600 < \nu < 5000 \text{ \AA}^{-1}$ (see Fig. 7) corresponds to wavelengths of $17 > \lambda > 2 \text{ \mu m}$. This suggests that the light should have been scattered by agglomerates the size of up to ≈ 20 μm formed by the much smaller

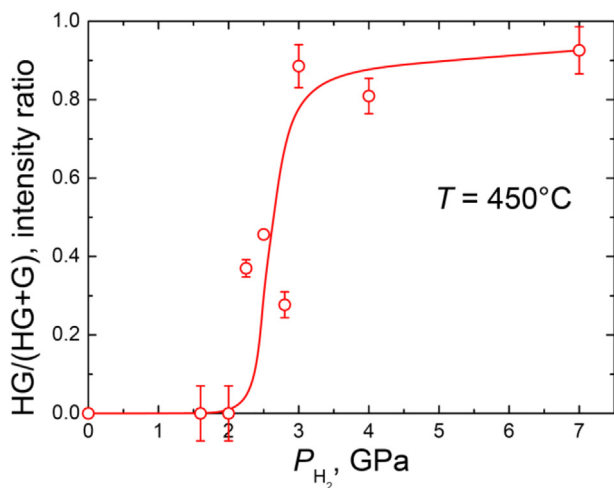


Fig. 6. The maximal ratio HG/(HG + G) of the integral intensities of the 002 lines of hydrographite (HG) and graphite (G) in the two-phase “graphite + hydrographite” samples synthesized by 24 h exposures of ball-milled graphite to an H₂ atmosphere at 450 °C and pressures indicated along the x-axis. (A colour version of this figure can be viewed online.)

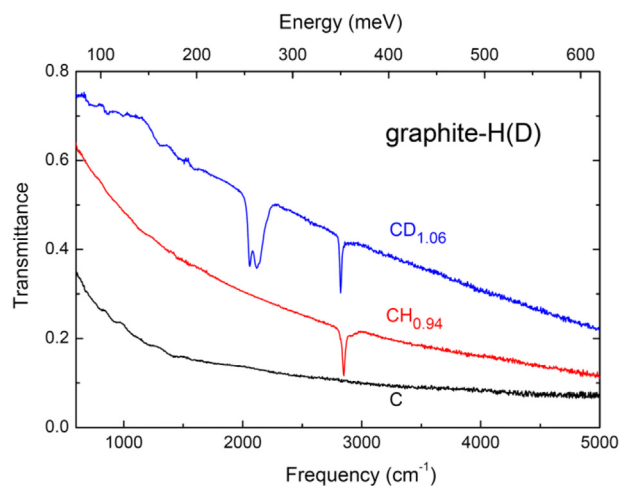


Fig. 7. IR transmission spectra, T(ν), of the ball-milled graphite powder (curve “C”) and the samples CH_{0.94} (synthesized at a hydrogen pressure of 7 GPa and T = 450 °C) and CD_{1.06} (synthesized at a deuterium pressure of 7.5 GPa and T = 450 °C). The absorption band near $\nu = 2820 \text{ cm}^{-1}$ in the CD_{1.06} spectrum is due to the H impurity in the sample. Bruker IFS-113v Fourier spectrometer, room temperature (Results of Ref. [7]). (A colour version of this figure can be viewed online.)

platelets of graphite or hydrographite, whose maximum dimension was about $0.4 \mu\text{m}$ (see Section 3.2).

We could not directly compare the sizes of the agglomerates of graphite and hydrographite platelets mixed with KBr in the samples studied by IR spectroscopy. However, the similarity in the spectral dependences $T(\nu)$ is indicative of similar sizes of the scattering particles (agglomerates) in the samples of the virgin and hydrogenated graphite. We therefore consider it most likely that the strong increase in the light transmittance by the hydrogenated graphite is mostly caused by the decrease in the intensity of the scattered light due to the lower conductivity of free charge carriers in hydrographite compared to graphite.

Such a conclusion agrees with results of *ab initio* calculations of the electronic structure of single layer and multilayer graphanes, all of them predicting an insulating or semiconducting behaviour of these materials (see Ref. [18] and references therein). The presence of the impurity of highly conductive graphite in the $\text{CH}_{0.94}$ sample can explain (at least, partly) its smaller light transmittance compared to the single-phase $\text{CD}_{1.06}$ sample.

In order to analyze the narrow absorption bands observed in the IR spectra of hydrogenated graphite samples in the range of the C–H and C–D stretching vibrations, transmittance $T(\nu)$ of a few samples was first formally converted to absorption defined as $A^*(\nu) = -\ln(T)$. From these $A^*(\nu)$ spectra we then subtracted the monotonic “baselines” resulting predominantly from the light scattering discussed above. The $A(\nu)$ spectra thus obtained are shown in Figs. 8 and 9 and expected to mostly represent the light absorption due to the excited stretching vibrations of the C–H and C–D bonds.

According to the *ab initio* calculations, the C–H stretching vibrations in a single-layer graphane [14,21] and a multilayer graphane [18] in the chair conformation should form a narrow band far above the bands of other vibrations, in the range $2830 < \nu < 2890 \text{ cm}^{-1}$ [14,18] or $2730 < \nu < 2780 \text{ cm}^{-1}$ [21]. The position $\nu \approx 2850 \text{ cm}^{-1}$ of the main peak in the absorption band of the $\text{CH}_{0.94}$ sample (bottom panel of Fig. 8) well agrees with the calculations of Refs. [14,18]. However, this peak has a rather intense

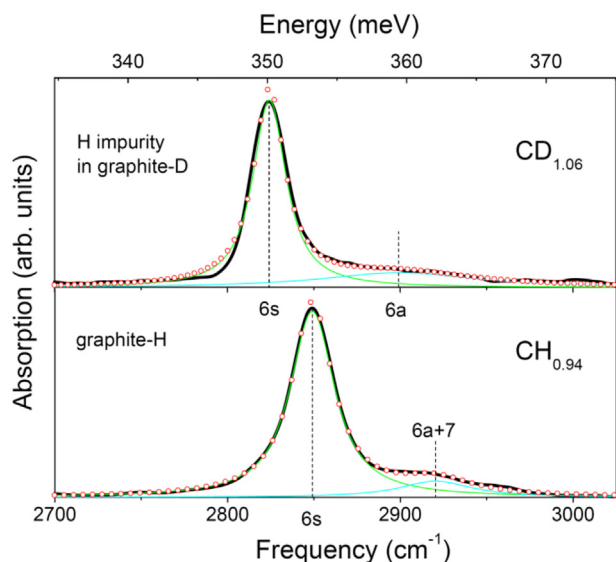


Fig. 8. IR absorption spectra, $A(\nu)$, of C–H stretching vibrations in the $\text{CH}_{0.94}$ sample (bottom panel) and $\text{CD}_{1.06}$ sample (top panel, modes due to the H impurity). Thick solid lines represent the experimental spectra; thin solid lines show a deconvolution of these spectra to Lorentzians; chains of open circles embody the Lorentzians; vertical dashed lines indicate the centers of the Lorentzians. The bands are numbered as in Table 2. (A colour version of this figure can be viewed online.)

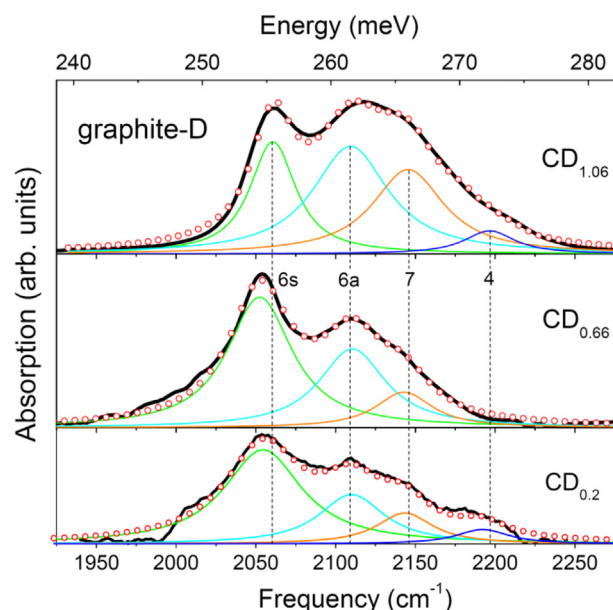


Fig. 9. IR absorption spectra, $A(\nu)$, of C–D stretching vibrations in three samples of deuterated graphite with different mean deuterium concentrations resulted from the different proportions between the unreacted graphite and hydrographite with the composition close to CD. The lines have the same meaning as in Fig. 8. The bands are numbered as in Table 2. (A colour version of this figure can be viewed online.)

shoulder extending up to 2980 cm^{-1} that contradicts the calculations. The absorption band of the $\text{CD}_{1.06}$ sample (upper panel of Fig. 9) is even broader. It clearly shows a complex fine structure and its intensity distribution considerably differs from that in the C–H band of the $\text{CH}_{0.94}$ sample.

These findings led us to think that the light penetration depth into our samples could be very small, and instead of the light absorption by the regular crystal structure in the bulk of the samples, we only observed results of the light scattering by various defect states on the sample surface.

An accurate analysis of stretching absorption bands of possible surface carbon-hydrogen configurations and their comparison with the deconvoluted bands in the experimental IR spectra of amorphous hydrogenated carbon thin films were carried out in Ref. [33]. The results of that work are presented in columns 1–4 of Table 2. The experiment confirmed the presence of 4 different types of stretching vibrations of CH groups (bands 1, 2, 4 and 7) and 2 types of vibrations of CH_2 groups (bands 6a and 6s), with coinciding frequency ranges of bands 7 and 6a. One could expect that the surface layers of our samples, which were considerably disturbed by the preliminary ball-milling, reacted with hydrogen similarly to the amorphous films therefore producing the same C–H groups vibrating in the same way as in Ref. [33].

A deconvolution of the overlapping absorption bands in our $\text{CH}_{0.94}$ sample into two Lorentzians is depicted in Fig. 8 (bottom panel) by thin lines. The positions and widths of these Lorentzians are indicated in column 5 of Table 2. As one can see, the two deconvoluted bands thus obtained are bands 6s and (6a+7) predicted in Ref. [33] and having the maximum integral intensities in the IR spectra of amorphous hydrogenated carbon films studied experimentally [33].

The band of stretching C–D vibrations in the $\text{CD}_{1.06}$ sample can be deconvoluted into 4 Lorentzians (see the upper panel in Fig. 9). To check if the deconvolution is meaningful, we also measured and deconvoluted spectra of two other samples of deuterated graphite, $\text{CD}_{0.66}$ and $\text{CD}_{0.20}$, containing, respectively, about 34 and 80 mol.% of

Table 2
Deconvoluted C–H and C–D stretching absorption bands. Columns 1–4 are from Ref. [33] and present the configuration (2) and predicted (3) and experimental (4) frequencies of CH_n groups (n = 1, 2, 3) at the surface of hydrogenated amorphous carbon films. The di- and trihydrogen bands are doublets with a “symmetric” (s) and “antisymmetric” (a) vibration. Frequencies in column 6 are for the deuterium-substituted configurations from column 2 calculated in a harmonic approximation using frequencies from column 3. Columns 5, 7 and 8 show experimental results for the CH_{0.94} and CD_{1.06} samples of crystalline hydrographite studied in the present paper. All experimental results are presented in the form “peak frequency/halfwidth” of the corresponding Lorentzian.

Band No [33].	Configuration [33]	Predicted C–H bands [33] (cm ⁻¹)	C–H bands in amorphous carbon [33] (cm ⁻¹)	C–H bands in CH _{0.94} (cm ⁻¹)	Predicted C–D bands (cm ⁻¹)	C–D bands in CD _{1.06} (cm ⁻¹)	C–H impurity bands in CD _{1.06} (cm ⁻¹)
1	2	3	4	5	6	7	8
1	sp ¹ CH	3305	3300/44	–	2427	–	–
2	sp ² CH(arom.)	3050	3045/68	–	2239	–	–
3a	sp ² CH ₂ (olef.)	3020	–	–	–	–	–
4	sp ² CH(olef.)	3000	3000/78	–	2203	~2200/27	–
5a	sp ³ CH ₃ (asym.)	2960	–	–	–	–	–
3s	sp ² CH ₂ (olef.)	2950	–	–	–	–	–
6a	sp ³ CH ₂ (asym.)	2925	2920/88	2920/25	2110	2109/27	~2900/40
7	sp ³ CH	2915	2920/88	2920/25	2140	2146/20	?
5s	sp ³ CH ₃ (sym.)	2870	–	–	–	–	–
6s	sp ³ CH ₂ (sym.)	2855	2850/78	2849/15	2060	2060/15	2824/8

unreacted graphite. As one can see from Fig. 9, the positions and widths of the Lorentzians are rather well reproduced in all three spectra, the only exception being the Lorentzian at ~2197 cm⁻¹ missing in the spectrum of the CD_{0.66} sample.

To assign the obtained frequencies to particular carbon-deuterium configurations, we calculated the frequencies of stretching vibrations of the CD and CD₂ groups in a harmonic approximation by dividing the predicted frequencies for the CH and CH₂ groups (column 3) by a square root of the corresponding ratio of the reduced masses, $\sqrt{M_{CD}/M_{CH}} \approx 1.362$ or $\sqrt{M_{CD_2}/M_{CH_2}} \approx 1.386$. The reduced masses were determined from equations $1/M_{CH} = 1/m_C + 1/m_H$ and $1/M_{CH_2} = 1/m_C + 2/m_H$ and analogous equations for the deuterium-substituted groups, using the atomic masses m_C , m_H and m_D of carbon, protium and deuterium.

The calculated frequencies for the CD and CD₂ groups are given in column 6 of Table 2 and allow unequivocal assignments of all four deconvoluted bands of stretching C–D vibrations in the CD_{1.06} sample (column 7). Note that band 7 lies slightly lower than band 6a in the carbon-protium spectra (column 3), but has a considerably higher frequency than band 6a in the carbon-deuterium spectra (column 6). Since the effect is due to the different isotopic dependences of frequencies of stretching vibrations of the CH and CH₂ groups, the agreement between the calculated and experimental frequencies for band 7 additionally confirms that the assignments of the deconvoluted C–D bands (column 7) are correct. The occurrence of band 7 detached from band 6a in the C–D spectra also partly explains the striking difference in the intensity distribution in the C–D and C–H spectra of the deuterated and hydrogenated graphite.

There is, however, another feature of stretching vibrations in hydrographite that we cannot explain at the moment. As one can see from the bottom panel of Fig. 8, the integral intensity of bands (6a+7) located at 2920 cm⁻¹ is much lower than that of band 6s at 2850 cm⁻¹. At the same time, the frequencies ($\nu_{6a} \approx 2925$ cm⁻¹ and $\nu_{6s} \approx 2855$ cm⁻¹) and relative intensities ($I_{6a}/I_{6s} \approx 3/1$) of bands 6a and 6s of antisymmetric and symmetric stretching vibrations of methylene groups CH₂ are known to experience little changes in nearly all atomic environments (see, e.g., Ref. [34] and references therein). Particularly, experiment gave $I_{6a} \gg I_{6s}$ for the amorphous hydrogenated carbon films [33].

So far as the I_{6a}/I_{6s} ratio is concerned, the samples of hydrogenated graphite considerably differ even from the deuterated samples. In the IR spectra of deuterated graphite shown in Fig. 9, band 6a has a higher integral intensity than band 6s in the single-phase sample CD_{1.06} and a smaller but comparable intensity in the two-

phase samples CD_{0.66} and CD_{0.2}. The intensity of band 7 of stretching vibrations of the methylylidene CD groups is smaller but comparable with the intensity of band 6s in all three C–D samples. In contrast, our nearly single-phase CH_{0.94} sample has $I_{(6a+7)}/I_{6s} \approx 1/7$ (this result, however, can only be considered as an estimate by the order of magnitude in view of the uncertainty in the smooth “baseline” subtracted from the experimental IR spectrum in order to isolate the A(ν) spectrum of stretching vibrations).

The last thing to be discussed in this Section is the stretching vibrations resulting from the presence of H impurity in the CD_{1.06} sample of deuterated graphite. As seen from Fig. 8, the spectrum of these vibrations (top panel) looks similar to the spectrum of stretching vibrations in the isotopically pure CH_{0.94} sample (bottom panel) shifted by ≈ 25 cm⁻¹ to lower frequencies. Results of deconvolution of the impurity spectrum into two Lorentzians are shown in Fig. 8 by the thin solid lines and presented in the last column of Table 2. The ratio of the integral intensities of the Lorentzians is of the order of 1/3.

Since the CD_{1.06} sample was synthesized in an atmosphere of the gas with an atomic ratio of H/D ≈ 0.03 , it is reasonable to expect that the sample also had H/D $\ll 1$. Consequently, the impurity spectrum should mostly be composed of stretching bands of CH and CDH groups, because the probability of formation of CH₂ groups was smaller than that of the CHD groups approximately by a factor of (H/D). Irrespective of the atomic environment, the bands of stretching vibrations of the CHD group are known to little differ in frequency and relative intensity from the antisymmetric and symmetric stretching bands of the CH₂ groups, and only the width of the symmetric band noticeably decreases (see, e.g., Ref. [34] where these features of the CHD vibrations were demonstrated on the example of isotopically isolated n-C₃₆H₇₄ chains in an n-C₃₆D₇₄ crystal). This is exactly as the H impurity spectrum of the CD_{1.06} sample looks like, including the narrowing of the 6s band. The presence of band 7 of stretching vibrations of the impurity CH groups in the deuterated sample is also likely, because this would explain the large half-width of the deconvoluted impurity 6a band (40 cm⁻¹ compared to 25 cm⁻¹ in the CH_{0.94} sample) and the smaller decrease in its frequency compared to the impurity 6s band (by 20 and 25 cm⁻¹, respectively) relative to the frequencies of bands 6a and 6s in the spectrum of the CH_{0.94} sample (see Table 2).

4. Conclusions

Summarizing the obtained results, the properties of hydrographite can be described as follows:

- Hydrographite is a solid black compound with the composition close to CH. This compound can be synthesised by exposing graphite to an atmosphere of molecular hydrogen at $P > 2$ GPa and $450 < T < 700$ °C. The yield of the reaction increases, if the surface of the graphite is activated by ball milling.
- Hydrographite is thermally stable under ambient conditions. If heated in vacuum, it decomposes to graphite and H₂ gas in the temperature interval from approx. 500 to 650 °C. Heating above 720–750 °C in an H₂ gas compressed to 7.5 GPa transforms hydrographite to methane and/or other light hydrocarbons.
- Hydrographite has a hexagonal crystal structure with the lattice parameters $a = 2.53(1)$ Å and $c = 9.54(1)$ Å and the volume $V = \frac{\sqrt{3}}{2}a^2c = 52.9(4)$ Å³/atom C. These values are larger than those of graphite by, respectively, 2.4(2) and 42.0(3) and 49(2)%.
- Comparison of the X-ray diffraction results with the available *ab initio* calculations suggests that hydrographite should be a 3D counterpart of graphane. Of the two most stable polytypes predicted for multilayer graphane [18], only the “graphane II” structure is compatible with experiment. This structure belongs to the P6₃mc space group and consists of one-layer sheets of graphane in the chair conformation stacked along the c axis in the –ABAB– sequence.
- Infrared spectroscopy revealed an anomalously small ratio of integral intensities of the bands of antisymmetric and symmetric stretching vibrations of CH₂ groups on the surface of hydrographite particles. This distinguishes hydrographite from other hydrocarbons.

Acknowledgements

The work was supported by Grant No. 11-02-00401 from the Russian Foundation for Basic Research and by the Program “The Matter under High Pressure” of the Russian Academy of Sciences. A.I.K. greatly acknowledges the support from the Scientific User Facilities Division, Office of Basic Energy Sciences, US Department of Energy.

References

- [1] H.P. Scott, R.J. Hemley, H.K. Mao, D.R. Herschbach, L.E. Fried, W.M. Howard, S. Bastea, Generation of methane in the Earth's mantle: in situ high pressure–temperature measurements of carbonate reduction, *Proc. Nat. Acad. Sci. U. S. A.* 101 (39) (2004) 14023–14026.
- [2] V.G. Kutcherov, A.Y. Kolesnikov, T.I. Dyuzheva, L.F. Kulikova, N.N. Nikolaev, O.A. Sazanova, V.V. Braghkin, Synthesis of complex hydrocarbon systems at temperatures and pressures corresponding to the Earth's upper mantle conditions, *Dokl. Phys. Chem.* 433 (1) (2010) 132–135.
- [3] V. Kutcherov, A. Kolesnikov, T. Dyuzheva, V. Brazhkin, Synthesis of hydrocarbons under upper mantle conditions: evidence for theory of abiotic deep petroleum origin, *J. Phys. Conf. Ser.* 215 (012103) (2010) 1–8.
- [4] I.O. Bashkin, V.E. Antonov, A.V. Bazhenov, I.K. Bdikin, D.N. Borisenko, E.P. Krinichnaya, et al., Thermally stable hydrogen compounds obtained under high pressure on the basis of carbon nanotubes and nanofibers, *JETP Lett.* 79 (5) (2004) 226–230.
- [5] A.C. Dillon, M.J. Heben, Hydrogen storage using carbon adsorbents: past, present and future, *Appl. Phys. A* 72 (2) (2001) 133–142.
- [6] S. Orimo, G. Majer, T. Fukunaga, A. Züttel, L. Schlapbach, H. Fujii, Hydrogen in the mechanically prepared nanostructured graphite, *Appl. Phys. Lett.* 75 (20) (1999) 3093–3095.
- [7] I.O. Bashkin, V.E. Antonov, A.V. Bazhenov, T.N. Fursova, R.V. Lukashev, M.K. Sakharov, et al., High-pressure hydrogenation of graphite, in: *Extended abstracts, X internat. conf. “Hydrogen Materials Science and Chemistry of Carbon Nanomaterials” ICHMS'2007. Sudak (Ukraine), 2007*, pp. 686–687.
- [8] K.S. Novoselov, A.K. Geim, S.V. Morozov, D. Jiang, Y. Zhang, S.V. Dubonos, et al., Electric field effect in atomically thin carbon films, *Science* 306 (2004) 666–669.
- [9] A.K. Geim, K.S. Novoselov, The rise of graphene, *Nat. Mater.* 6 (2007) 183–191.
- [10] M.H.F. Sluiter, Y. Kawazoe, Cluster expansion method for adsorption: application to hydrogen chemisorption on graphene, *Phys. Rev. B* 68 (085410) (2003) 1–7.
- [11] J.O. Sofo, A.S. Chaudhari, G.D. Barber, Graphane: A two-dimensional hydrocarbon, *Phys. Rev. B* 75 (153401) (2007) 1–4.
- [12] D.C. Elias, R.R. Nair, T.M.G. Mohiuddin, S.V. Morozov, P. Blake, M.P. Halsall, et al., Control of graphene's properties by reversible hydrogenation: evidence for graphane, *Science* 323 (2009) 610–613.
- [13] V.I. Artyukhov, L.A. Chernozatonskii, Structure and layer interaction in carbon monofluoride and graphane: A comparative computational study, *J. Phys. Chem. A* 114 (16) (2010) 5389–5396.
- [14] E. Cadelano, P.L. Palla, S. Giordano, L. Colombo, Elastic properties of hydrogenated graphene, *Phys. Rev. B* 82 (235414) (2010) 1–8.
- [15] G. Savini, A.C. Ferrari, F. Giustino, First-principles prediction of doped graphane as a high-temperature electron-phonon superconductor, *Phys. Rev. Lett.* 105 (037002) (2010) 1–4.
- [16] A.A. Dzhurakhalov, F.M. Peeters, Structure and energetics of hydrogen chemisorbed on a single graphene layer to produce graphane, *Carbon* 49 (10) (2011) 3258–3266.
- [17] D.K. Samarakoon, X.-Q. Wang, Chair and twist-boat membranes in hydrogenated graphene, *ACS Nano* 3 (12) (2009) 4017–4022.
- [18] X.-D. Wen, L. Hand, V. Labet, T. Yang, R. Hoffmann, N.W. Ashcroft, et al., Graphane sheets and crystals under pressure, *Proc. Nat. Acad. Sci. U. S. A.* 108 (17) (2011) 6833–6837.
- [19] J. Rohrer, P. Hylgaard, Stacking and band structure of van derWaals bonded graphane multilayers, *Phys. Rev. B* 83 (165423) (2011) 1–10.
- [20] O. Leenaerts, H. Peelaers, A.D. Hernández-Nieves, B. Partoens, F.M. Peeters, First-principles investigation of graphene fluoride and graphane, *Phys. Rev. B* 82 (195436) (2010) 1–6.
- [21] H. Peelaers, A.D. Hernández-Nieves, O. Leenaerts, B. Partoens, F.M. Peeters, Vibrational properties of graphene fluoride and graphane, *Appl. Phys. Lett.* 98 (051914) (2011) 1–3.
- [22] D.W. Boukhvalov, M.I. Katsnelson, A.I. Lichtenstein, Hydrogen on graphene: electronic structure, total energy, structural distortions and magnetism from first-principles calculations, *Phys. Rev. B* 77 (035427) (2008) 1–7.
- [23] V.E. Antonov, I.O. Bashkin, S.S. Khasanov, A.P. Moravsky, Y.G. Morozov, Y.M. Shulga, et al., Magnetic ordering in hydrofullerite C₆₀H₂₄, *J. Alloys Comp.* 330–332 (2002) 365–368.
- [24] L.G. Khvostantsev, V.N. Slesarev, V.V. Brazhkin, Toroid type high-pressure device: history and prospects, *High. Press. Res.* 24 (2004) 371–383.
- [25] V.E. Antonov, A.I. Davydov, V.K. Fedotov, A.S. Ivanov, A.I. Kolesnikov, M.A. Kuzovnikov, Neutron spectroscopy of H impurities in PdD: covibrations of the H and D atoms, *Phys. Rev. B* 80 (13) (2009), 134302(1–7).
- [26] A.I. Kolesnikov, I.O. Bashkin, V.E. Antonov, D. Colognesi, J. Mayers, A.P. Moravsky, Neutron spectroscopy study of single-walled carbon nanotubes hydrogenated under high pressure, *J. Alloys Comp.* 446–447 (2007) 389–392.
- [27] Y.M. Shul'ga, I.O. Bashkin, A.V. Krestinin, V.M. Martynenko, G.I. Zvereva, I.V. Kondrat'eva, et al., Spectrum of gases liberated upon the stepwise heating of single-walled carbon nanotubes deuterated under pressure, *JETP Lett.* 80 (12) (2004) 752–756.
- [28] S. Orimo, T. Matsushima, H. Fujii, T. Fukunaga, G. Majer, Hydrogen desorption property of mechanically prepared nanostructured graphite, *J. Appl. Phys.* 90 (3) (2001) 1545–1549.
- [29] T. Fukunaga, K. Nagano, U. Mizutani, H. Wakayama, Y. Fukushima, Structural change of graphite subjected to mechanical milling, *J. Non Cryst. Solids* 232–234 (1998) 416–420.
- [30] Y. Chen, J.F. Gerald, L.T. Chadderton, L. Chaffron, Nanoporous carbon produced by ball milling, *Appl. Phys. Lett.* 74 (19) (1999) 2782–2784.
- [31] R.A. Friedel, G.L. Carlson, Infrared spectra of ground graphite, *J. Phys. Chem.* 75 (8) (1971) 1149–1151.
- [32] M. Born, E. Wolf, *Principles of Optics*, fourth ed., Pergamon, Oxford, 1968.
- [33] B. Dischler, A. Bubenzer, P. Koidl, Bonding in hydrogenated hard carbon studied by optical spectroscopy, *Solid State Commun.* 48 (2) (1983) 105–108.
- [34] R.G. Snyder, S.L. Hsu, S. Krimm, Vibrational spectra in the C–H stretching region and the structure of the polymethylene chain, *Spectrochim. Acta* 34A (1978) 395–406.